

Cite this: *Mater. Adv.*, 2021,  
2, 6278Received 22nd July 2021,  
Accepted 3rd September 2021

DOI: 10.1039/d1ma00636c

rsc.li/materials-advances

## Fluorescence and biological stabilization of phosphorus-functionalized mesoporous silica nanospheres modified with a bis(8-hydroxyquinoline) zinc complex†

Norio Saito,<sup>ib</sup>\*<sup>a</sup> Daichi Noda,<sup>b</sup> Yucheng Shang,<sup>b</sup> Shota Yamada<sup>b</sup> and Motohiro Tagaya<sup>ib</sup><sup>b</sup>

**Green-emitting phosphorus-functionalized mesoporous silica (PMPS) nanospheres were fabricated by modifying their surfaces with (8-hydroxyquinoline) zinc (Znq<sub>2</sub>). A simulated body fluid soaking test and subsequent gas-adsorption measurements revealed that Znq<sub>2</sub>-modification could dramatically suppress the biodegradation of the nanospheres. This study establishes Znq<sub>2</sub> as a novel and potential surface modifier of mesoporous silicas and demonstrates that effective surface design of the hosts will allow the exploitation of potential functionalities of the modifier.**

Ordered porous materials such as metal organic frameworks (MOFs), zeolites, and mesoporous silicas (MPSs) have been widely investigated as unique hosts that can incorporate organic molecules and inorganic clusters into well-defined nanospaces.<sup>1</sup> In particular, MPSs are promising nanoporous hosts with a large surface area and a uniform and adjustable pore structure, allowing facile modification on their internal and external surfaces with metal ions and functional molecules.<sup>2</sup> They have been utilized for biomedical applications,<sup>3</sup> catalytic processes,<sup>4</sup> and adsorption-based applications.<sup>5</sup>

Metal 8-hydroxyquinolinate complexes such as tris(8-hydroxyquinoline)aluminum (Alq<sub>3</sub>) and their related derivatives are known to be typical optoelectronic building blocks.<sup>6</sup> This class of molecules effectively interacts with nanoporous materials and is easily immobilized on their surfaces through chemical adsorption.<sup>7</sup> It is worth noting that molecular assembly in such small nanospaces restricts the conformation of the guest molecule and induces unique guest–guest and/or host–guest interactions. This, in turn, leads to the emergence of

optoelectronic properties that are not exhibited in solutions and bulk crystals. For instance, Fazaeli *et al.* demonstrated that compared to the case of bulk  $\alpha$ -Alq<sub>3</sub> crystal, covalent grafting of Alq<sub>3</sub> and its substituent molecules on the MPS surface resulted in a significant blue shift of the fluorescence due to changes in the coordination environment of the Al<sup>3+</sup> center.<sup>8</sup> Similarly, Du *et al.* successfully synthesized (8-hydroxyquinoline) zinc (Znq<sub>2</sub>)-modified MPSSs and observed a significant blue shift of their greenish fluorescence when the host surface was functionalized with mercapto and sulfonic acid groups.<sup>9</sup> These studies suggest that the optical properties of Alq<sub>3</sub> and Znq<sub>2</sub> can be modulated through assembly in the nanospaces of MPSSs and through their interface functionalization.

In this study, we have prepared phosphorus-containing MPS (PMPS) nanospheres using diethyl(2-bromoethyl)phosphonate as a phosphorus source.<sup>10</sup> The mesoporous channels of PMPS were modified with Znq<sub>2</sub>. Adsorption experiments revealed that Znq<sub>2</sub> was more favorably adsorbed on the PMPS surface than the case on the MPS surface. Interestingly, Znq<sub>2</sub> modification of the PMPS surface efficiently prevented its anionic component dissolution from the surface of the mesopores into the simulated body fluid (SBF). Additionally, it was revealed that Znq<sub>2</sub> could be utilized as a surface modifier that could induce fluorescence and biological stability as the host functionalities.

The MPS and PMPS nanospheres were synthesized according to our previously reported method.<sup>10</sup> For synthesizing PMPS, the phosphorus to silica (P/Si) molar ratio was set to 6 (*i.e.*, P/Si = 6) by adjusting the amounts of the silicate and phosphorus sources. Adsorption of Znq<sub>2</sub> into the prepared nanospheres was induced by admixing the nanospheres and an ethanol solution of Znq<sub>2</sub> of several initial concentrations (*n*) ranging from 0.15 to 0.75 mM. The resulting particles were washed with ultrapure water and dried under reduced pressure for 24 h. The Znq<sub>2</sub>-modified MPS and PMPS were designated as *n*Z/MPS and *n*Z/PMPS, respectively, where *n* indicates the concentration of Znq<sub>2</sub> used for the chemisorption experiments. For the synthesis of PMPS, the phosphorus source diethyl

<sup>a</sup> Department of Industrial Chemistry, Faculty of Engineering, Tokyo University of Science, 1-3 Kagurazaka, Shinjuku, Tokyo 162-8601, Japan. E-mail: nsaito@rs.tus.ac.jp

<sup>b</sup> Department of Materials Science and Technology, Nagaoka University of Technology, Kamitomioka 1603-1, Nagaoka, Niigata 940-2188, Japan

† Electronic supplementary information (ESI) available. See DOI: 10.1039/d1ma00636c



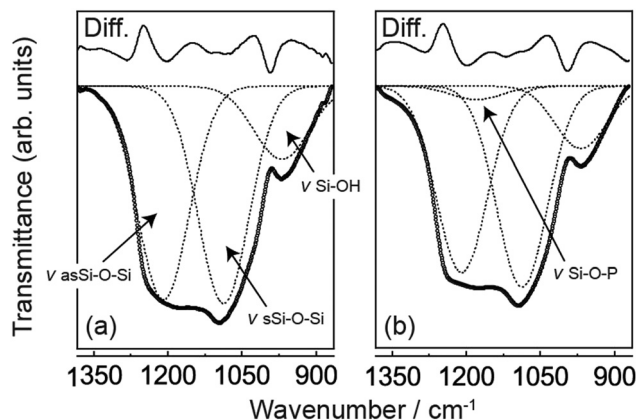


**Fig. 1** FT-IR spectra of (a) MPS and (b) PMPS in the siliceous bonding region. The open circles show observed spectra, and the dotted lines are simulated ones obtained by the deconvolution calculations. The top solid lines mean differences between the observed and simulated spectra. In spectrum (a), the observed signal was deconvoluted into three characteristic peaks assignable to a couple of Si–O–Si asymmetric and symmetric stretching vibrations and Si–OH stretching vibrations and Si–O–Si bonds. In spectrum (b), a new hump was observed at  $1174\text{ cm}^{-1}$ , assignable to the Si–O–P stretching vibration.

(2-bromoethyl)phosphonate was hydrolyzed together with the hydrolysis reaction of tetraethyl orthosilicate.

The hydrolyzed phosphorus source interacts with the surface of the MPS precursor *via* the hydrogen bonding of the hydroxyl groups, followed by Si–O–P bond formation *via* the dehydrated condensation between their hydroxyl groups. Subsequent calcination led to decomposition of the bromoethyl moiety of the phosphorus source,<sup>11</sup> and thus, the phosphate group was retained on the surface of the silicate framework. As discussed later, these functional groups strongly enhanced  $\text{Znq}_2$  adsorption on the PMPS surface. Details of the synthesis procedures are described in the ESI.†

Fourier transform infrared (FT-IR) spectroscopy of MPS and PMPS was performed to ascertain if phosphorus was introduced into the polysiloxane covalent framework. Fig. 1 shows the FT-IR spectra of MPS and PMPS in the range of the siliceous bonding region. Results of the peak deconvolution analysis are also shown in this figure. Total differences between the calculated and observed spectra were 5.0% for MPS and 6.3% for PMPS, suggesting that the sum of the deconvoluted peaks well reproduced the observed data. The spectra of MPS (Fig. 1a) show three shoulder-like peaks at  $1204$ ,  $1092$ , and  $969\text{ cm}^{-1}$ , and the peak deconvolution analysis revealed that these peaks are assignable to a couple of Si–O–Si asymmetric and symmetric stretching vibrations and Si–OH stretching vibrations.<sup>12</sup> On the other hand, in the case of PMPS (Fig. 1b), a new hump was observed at  $1174\text{ cm}^{-1}$ , corresponding to the Si–O–P stretching vibration.<sup>13</sup> This indicated that a significant amount of phosphorus was successfully introduced into PMPS.

The prepared MPS and PMPS were modified with  $\text{Znq}_2$  through chemisorption, and their gas-adsorption properties were examined using  $\text{N}_2$  adsorption/desorption experiments. The adsorption/desorption isotherms suggested apparently different isotherm characteristics of  $n\text{Z}/\text{MPS}$  and  $n\text{Z}/\text{PMPS}$  (Fig. S1, ESI†).

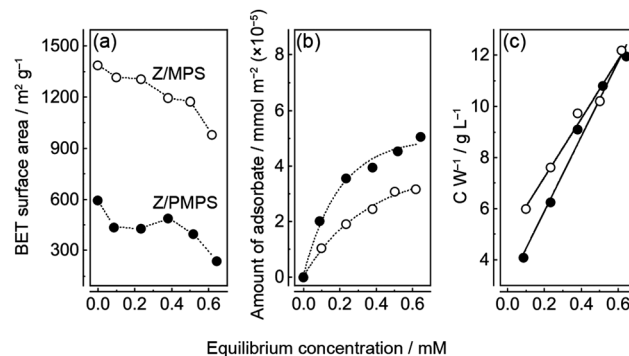


**Fig. 2** (a) Variation in the  $S_{\text{BET}}$  values of  $n\text{Z}/\text{MPS}$  and  $n\text{Z}/\text{PMPS}$  and the equilibrium adsorption concentration measured in the chemisorption experiments. (b) Equilibrium adsorption isotherms of  $\text{Znq}_2$  obtained by the chemisorption experiments of MPS and PMPS.  $\text{Znq}_2$  was immobilized on the host surfaces by monolayered adsorption. (c) Scatchard plots of MPS and PMPS.

For all  $n$  values,  $n\text{Z}/\text{MPS}$  exhibited a type IV isotherm (Fig. S1a–e, ESI†) according to the IUPAC classification,<sup>14</sup> and their hysteresis loops exhibited complete reversibility. This suggested that  $n\text{Z}/\text{MPS}$  had cylindrical mesopores that were smaller than  $\approx 4\text{ nm}$ .<sup>15</sup> Indeed, low-angle powder X-ray diffraction (PXRD) measurements suggested that the wall thickness was approximately  $3\text{ nm}$  for  $n\text{Z}/\text{MPS}$  (Fig. S2a, ESI†). In contrast, the adsorption/desorption isotherms of  $n\text{Z}/\text{PMPS}$  (Fig. S1f–j, ESI†) showed characteristic desorption shoulders with lower closure points at  $0.42P_0$ ; additionally, a plateau at high  $P/P_0$  was absent. These features suggested H3-type hysteresis,<sup>15</sup> and possibly, an assembly of slit-shaped mesopores for  $n\text{Z}/\text{PMPS}$ . The PXRD profiles of  $n\text{Z}/\text{PMPS}$  indicated that the wall thickness of the slit-shaped mesopores was  $\approx 4\text{ nm}$  (Fig. S2b, ESI†).

Surface area analyses of  $n\text{Z}/\text{MPS}$  and  $n\text{Z}/\text{PMPS}$  (Fig. 2a) indicate that the latter had a smaller Brunauer–Emmett–Teller (BET) surface area ( $S_{\text{BET}}$ )<sup>16</sup> than the former due to the disordered mesopore distribution induced upon phosphorus incorporation into the polysiloxane framework.<sup>10</sup> Additionally, the  $S_{\text{BET}}$  value decreased slightly with increase in the equilibrium adsorption concentration of  $\text{Znq}_2$ , suggesting that  $\text{Znq}_2$  adsorption on the host surface closed a portion of their mesopore channels.

The amount of  $\text{Znq}_2$  loaded into the hosts was determined from the change in the visible absorbance of the  $\text{Znq}_2$  solution before and after the chemisorption experiments. The relation between the equilibrium concentration and the amount of adsorbate in the hosts suggested that  $\text{Znq}_2$  adsorption was consistent with a Langmuir type I isotherm.<sup>17</sup> Thus,  $\text{Znq}_2$  was immobilized in the nanospaces of the hosts *via* monolayer adsorption. Nevertheless, it must be noted that the surface of the mesoporous channels was not fully covered with  $\text{Znq}_2$ ; rather the surface coverage was remarkably low (discussed below) because the molecular size of  $\text{Znq}_2$  ( $\approx 1.5\text{ nm}$ )<sup>18</sup> is comparable to the size of the nanospaces in the hosts. The Scatchard plots (Fig. 2c) indicate that the maximum amounts of  $\text{Znq}_2$  ( $W_{\text{max}}$ ) loaded into MPS and PMPS were  $0.087$  and  $0.069\text{ mmol g}^{-1}$ , respectively. The difference could be



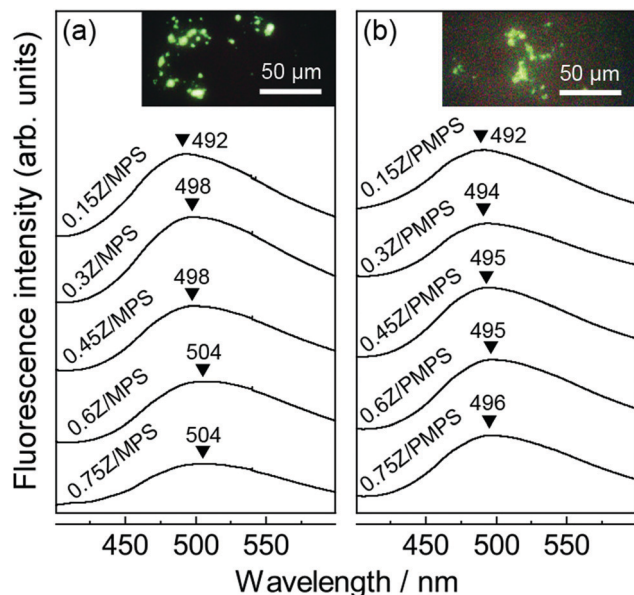


Fig. 3 Fluorescence spectra of (a) *n*Z/MPS and (b) *n*Z/PMPS. The insets show the fluorescence microscope images for *n* = 0.75 ( $\lambda_{\text{ex}}$  = 356 nm).

attributed to the higher  $S_{\text{BET}}$  value of *n*Z/MPS. The plots also suggest that the adsorption equilibrium constants ( $K_{\text{eq}}$ ) for *n*Z/MPS and *n*Z/PMPS were 2.3 and 4.9  $\text{M}^{-1}$ , respectively. This implies that  $\text{Znq}_2$  was more strongly immobilized on the PMPS surface than on the MPS surface. The favorable  $\text{Znq}_2$  immobilization on the PMPS surface was also confirmed by surface occupation analyses (Fig. S3, ESI<sup>†</sup>). Here, the surface occupation of  $\text{Znq}_2$  was estimated from the equilibrium adsorption amounts of the adsorbate and the  $S_{\text{BET}}$  values of the hosts. Consequently, the maximum surface occupation was calculated to be 2.2% for *n*Z/MPS and 3.4% for *n*Z/PMPS, implying a small but significant difference between their molecular immobilization capacities. The above results suggest that  $\text{Znq}_2$  should be more efficiently immobilized on the PMPS surface than on normal silicate surfaces.

Fig. 3 shows the fluorescence spectra of *n*Z/MPS and *n*Z/PMPS upon excitation at 356 nm. A broad, greenish emission centered around 500 nm, which is the characteristic  $\text{Znq}_2$  fluorescence, was observed.<sup>19</sup> Compared to the fluorescence spectrum of  $\text{Znq}_2$  recorded in the solid state or in ethanol (Fig. S4, ESI<sup>†</sup>), the spectra of *n*Z/MPS and *n*Z/PMPS exhibited apparently broadened emission and a large blue shift of more than 50 nm, clearly suggesting that the adsorption of the guest chromophores into the hosts could modulate their optical properties. Because the degree of the blue shift seemed to be more pronounced in the samples with less loaded  $\text{Znq}_2$  (Fig. 3a), it can be assumed that the interactions between  $\text{Znq}_2$  and the host surface were responsible for the optical modulation.

As mentioned before, the phosphate groups on the PMPS surface play an important role during adsorption to ensure the efficient immobilization of  $\text{Znq}_2$ . It should also be noted that the strong host-guest interaction in PMPS is likely to affect the optical properties of  $\text{Znq}_2$ . Indeed, Fig. 3b suggests that the

emission of *n*Z/PMPS was centered at almost a fixed wavelength in the range of 492–496 nm, while *n*Z/MPS exhibited a red shift from 492 to 504 nm with increase in the amount of loaded  $\text{Znq}_2$ . The fluorescence maxima of metal hydroxyquinoline complexes vary depending on their conformation and aggregation states, and particularly, the red shift in fluorescence can be attributed to the overlapping of the  $\pi$  orbitals of each quinoline ring.<sup>20</sup> Generally, the nanospaces in the hosts limit the conformational freedom of the guests and inhibit their aggregation.<sup>21</sup> On the other hand, for the case of *n*Z/MPS, a red shift in fluorescence was observed with increasing concentration of loaded  $\text{Znq}_2$ , indicating local molecular aggregation of  $\text{Znq}_2$ , possibly during the drying process. In contrast, the nearly constant fluorescence of *n*Z/PMPS suggests the immobilization of the  $\text{Znq}_2$  monomer. It is speculated that the PMPS surface mainly has two adsorption sites, *i.e.*, the negatively charged silanol ( $\text{Si-O}^-$ ) groups and the protonated phosphate ( $\text{O=P-OH}$ ) groups,<sup>22</sup> and that  $\text{Znq}_2$  interacts with these adsorption sites *via* electrostatic and hydrogen bonding interactions, respectively. We assume that the multi-point adsorption characteristic of the PMPS surface would inhibit the mobility and re-organization of  $\text{Znq}_2$ , thereby leading to fluorescence stabilization.

We examined the biological stability of the  $\text{Znq}_2$ -modified mesoporous hosts. For this experiment, we soaked MPS, PMPS, 0.75Z/MPS, and 0.75Z/PMPS in SBF at 36.5 °C, and then determined the concentrations of the  $\text{SiO}_3^{2-}$  anions dissolved in SBF using the molybdenum blue method,<sup>10</sup> since the dissolution rate of  $\text{SiO}_3^{2-}$  anions is an indicator of the degradation of silicate compounds. The sizes of the MPS and PMPS particles used in this experiment were 207 nm (cv. 9.1%) and 204 nm (cv. 8.6%), respectively.<sup>10</sup> Fig. 4a shows the time evolution of the  $\text{SiO}_3^{2-}$  concentration in the SBF; it is evident that the degradation of the host was significantly dependent on phosphorus incorporation and  $\text{Znq}_2$  modification. As seen in the figure, MPS shows rapid dissolution until 12 h, following which

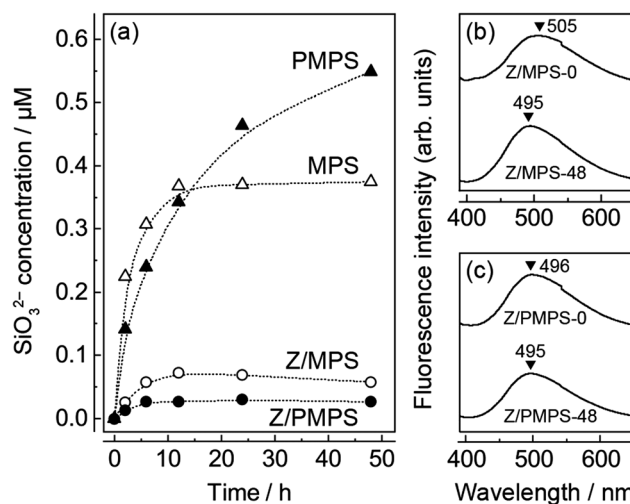


Fig. 4 (a) Time evolution of  $\text{SiO}_3^{2-}$  concentration after dissolution from MPS, PMPS, 0.75Z/MPS, and 0.75Z/PMPS in SBF. Fluorescence spectra of (b) 0.75Z/MPS and (c) 0.75Z/PMPS before and after SBF soaking.



an equilibrium state is attained. The total amount of the  $\text{SiO}_3^{2-}$  anions dissolved in 48 h from MPS was 2.8 wt%. The relatively low degradation rate was attributed to the condensation of the polysiloxane networks upon calcination.<sup>23</sup> PMPS also rapidly released the  $\text{SiO}_3^{2-}$  anions for the first 12 h; however, a plateau was not observed even after 48 h. The total amount of  $\text{SiO}_3^{2-}$  anions dissolved from PMPS was 4.2 wt%. Hence, PMPS is likely to be more prone to degradation in a biological environment. The rapid degradation of PMPS perhaps originates from the strong affinity between the PMPS surface and divalent metal cations. This hypothesis is rationalized by the fact that calcium phosphates were mineralized on the host surface after SBF soaking;<sup>10</sup> that is to say, adsorption of the  $\text{Ca}^{2+}$  cations on the host surface should be a triggering factor for  $\text{SiO}_3^{2-}$  dissolution and subsequent anionic compensation with ambient  $\text{HPO}_4^{2-}$ . In this reaction, the oxygen atoms of the hydroxyl and phosphate groups are assumed to predominantly behave as the reaction sites due to their strong ability to coordinate with the metal cations.<sup>24</sup> Indeed, we already reported that the PMPS surface forms a hydration layer having strong affinity with the hydrophilic protein molecules.<sup>25</sup> In addition, the functional groups on the PMPS surface are negatively charged at a neutral pH.<sup>25,26</sup> Hence, PMPS should have more active reaction sites with the metal cations than MPS, leading to the rapid degradation of the former host.

Fig. 4a also shows the  $\text{SiO}_3^{2-}$  dissolution behavior of the  $\text{Znq}_2$ -modified hosts. It is evident that surface modification dramatically reduced the amount of dissolved  $\text{SiO}_3^{2-}$  anions, possibly because of the enhanced surface hydrophobicity<sup>27</sup> and covering of the adsorption sites. One may be concerned that the  $\text{Znq}_2$  modification would deteriorate the solubility of MPS and PMPS in aqueous solutions. However, the  $\text{Znq}_2$  modification minimally affected the surface charge and solubility of the hosts, because  $\text{Znq}_2$  is preferentially immobilized in the nanospaces of the inner core due to the high density of the adsorptive groups in the nanospaces,<sup>28</sup> and the surface state of the outer shell is substantially identical to the unmodified ones. Since the total amounts of the dissolved  $\text{SiO}_3^{2-}$  anions were 0.45 and 0.21 wt% for 0.75Z/MPS and 0.75Z/PMPS, respectively, it can be concluded that the  $\text{Znq}_2$  modification rather stabilized the PMPS surface. The remarkable improvement in the biological stability of 0.75Z/PMPS was also confirmed from the  $\text{N}_2$  adsorption/desorption isotherms of the samples obtained after SBF soaking. The isotherms and their  $S_{\text{BET}}$  values (Fig. S5, ESI†) indicate that the adsorption properties of 0.75Z/PMPS did not change remarkably even after SBF soaking, which was in contrast to the significant decline of the adsorption volume observed for 0.75Z/MPS. The mesopore stability was also reflected in their fluorescence spectra (Fig. 4b and c), as the fluorescence emission maximum of 0.75Z/PMPS remained unchanged. Thus, we conclude that the  $\text{Znq}_2$  modification significantly improved the biological stability of the mesopores in PMPS because of the strong interface affinity between  $\text{Znq}_2$  and the PMPS surface.

In summary, we demonstrate a new concept of using  $\text{Znq}_2$  as a surface modifier that can induce greenish fluorescence and

biological stability of MPSS. We particularly highlight that the incorporation of phosphorus into the MPS surface allows the immobilization of monomeric  $\text{Znq}_2$  due to the strong affinity between  $\text{Znq}_2$  and the phosphate groups, further improving the biological stability of the host. Although there are reports on the modification of  $\text{Alq}_3$ ,  $\text{Znq}_2$ , and other complex molecules in the nanospaces of mesoporous hosts,<sup>8,9</sup> these studies were mainly focused on the optical and catalytic properties of the hybrids alone. In contrast, the present study focused on how the guest modification altered the properties of the host surface and demonstrates how effective interface design might be utilized to exploit the guest functions as well. We believe that the present concept will be especially useful in the development of biostable fluorescence markers and nanomedicines.

## Conflicts of interest

There are no conflicts to declare.

## Acknowledgements

This work was supported by JSPS KAKENHI Grant Number 21K14706. M. T. thanks Analysis and Instrumentation Center in Nagaoka University of Technology for providing the facilities.

## References

- P. Singh, S. Srivastava and S. K. Singh, *Sci. Eng.*, 2009, **5**, 4882; Y. Gao, D. Gao, J. Shen and Q. Wang, *Front. Chem.*, 2020, **8**, 598722.
- X. Feng, G. E. Fryxell, L. Q. Wang, A. Y. Kim, J. Liu and K. M. Kemner, *Science*, 1997, **276**, 923; D. Margolese, J. A. Melero, S. C. Christiansen, B. F. Chmelka and G. D. Stucky, *Chem. Mater.*, 2000, **12**, 2448; S. Chen, S. L. Greasley, Z. Y. Ong, P. Naruphontjirakul, S. J. Page, J. V. Hanna, A. N. Redpath, O. Tsigkou, S. Rankin, M. P. Ryan, A. E. Porter and J. R. Jones, *Mater. Today Adv.*, 2020, **6**, 100066.
- Q. Lei, J. Guo, A. Nouredine, A. Wang, S. Wuttke, C. J. Brinker and W. Zhu, *Adv. Funct. Mater.*, 2020, **30**, 1909539; M. Vallet-Regi, F. Balas and D. Arcos, *Angew. Chem., Int. Ed.*, 2007, **46**, 7548.
- M. Opanasenko, P. Stepnicka and J. Cejka, *RSC Adv.*, 2014, **4**, 65137.
- M. Kruk and M. Jaroniec, *Chem. Mater.*, 2001, **13**, 3169; M. Hartmann, *Chem. Mater.*, 2005, **17**, 4577.
- M. Albrecht, M. Fiege and O. Osetska, *Coord. Chem. Rev.*, 2008, **252**, 812; M. Amati, S. Belviso, P. L. Cristinziano, C. Minichino and F. Lelj, *J. Phys. Chem. A*, 2007, **111**, 13403.
- L.-N. Sun, H.-J. Zhang, J.-B. Yu, S.-Y. Yu, C.-Y. Peng, S. Dang, X.-M. Guo and J. Feng, *Langmuir*, 2008, **24**, 5500; A. Badiei, H. Goldoos and G. M. Ziarani, *Appl. Surf. Sci.*, 2011, **257**, 4912.
- Y. Fazaeli, M. M. Amini, E. Mohajerani, M. Sharbatdaran and N. Torabi, *J. Colloid Interface Sci.*, 2010, **346**, 384.
- Y. Du, Y. Fu, Y. Shi, X. Lü, C. Lü and Z. Su, *J. Solid State Chem.*, 2009, **182**, 1430.



- 10 Y. Shang, Y. Shota, Y. Chai and M. Tagaya, *Key Eng. Mater.*, 2019, **782**, 59; S. Yamada, Y. Shang, I. Yamada and M. Tagaya, *Adv. Powder Technol.*, 2019, **30**, 1116.
- 11 Y. Okamoto, T. Kawai and H. Sakurai, *Bull. Chem. Soc. Jpn.*, 1974, **47**, 2903.
- 12 E. I. Kamitsos and A. P. Patsis, *Phys. Rev. B: Condens. Matter Mater. Phys.*, 1993, **48**, 12499; E. Astorino, J. B. Peri, R. J. Willey and G. Busca, *J. Catal.*, 1995, **157**, 482.
- 13 L. Todan, C. Andronescu, D. M. Vuluga, D. C. Culita and M. Zaharescu, *J. Therm. Anal. Calorim.*, 2013, **114**, 91.
- 14 M. Thommes, K. Kaneko, A. V. Neimark, J. P. Olivier, F. Rodriguez-Reinoso, J. Rouquerol and K. S. W. Sing, *Pure Appl. Chem.*, 2015, **87**, 1051.
- 15 K. A. Cychoz, R. Guillet-Nicolas, J. Garcia-Martinez and M. Thommes, *Chem. Soc. Rev.*, 2017, **46**, 389.
- 16 S. Brunauer, P. H. Emmett and E. Teller, *J. Am. Chem. Soc.*, 1938, **60**, 309.
- 17 I. Abe, *J. Oleo Sci.*, 2002, **2**, 275.
- 18 L. S. Sapochak, F. E. Benincasa, R. S. Schofield, J. L. Baker, K. K. C. Riccio, D. Fogarty, H. Kohlmann, K. F. Ferris and P. E. Burrows, *J. Am. Chem. Soc.*, 2002, **124**, 6119.
- 19 S. Li, J. Lu, H. Ma, D. Yan, Z. Li, S. Qin, D. G. Evans and X. Duan, *J. Phys. Chem. C*, 2012, **116**, 12836; H.-C. Pan, F.-P. Liang, C.-J. Mao, J.-J. Zhu and H.-Y. Chen, *J. Phys. Chem. B*, 2007, **111**, 5767.
- 20 M. Brinkmann, G. Gadret, M. Muccini, C. Taliani, N. Masciocchi and A. Sironi, *J. Am. Chem. Soc.*, 2000, **122**, 5147.
- 21 T. Azaïs, C. Tourné-Péteilh, F. Aussenac, N. Baccile, C. Coelho, J.-M. Devoisselle and F. Babonneau, *Chem. Mater.*, 2006, **18**, 6382.
- 22 D. Singappuli-Arachchige and I. I. Slowing, *J. Chem. Phys.*, 2020, **152**, 034703; R. Liu, L. Chi, X. Wang, Y. Sui, Y. Wang and H. Arandiyán, *J. Environ. Chem. Eng.*, 2018, **6**, 5269.
- 23 J. G. Croissant, Y. Fatieiev and N. M. Khashab, *Adv. Mater., Microporous Mesoporous Mater.*, 2010, **131**, 314.
- 24 O. Francesconi, M. Gentili, F. Bartoli, A. Bencini, L. Conti, C. Giorgi and S. Roelens, *Org. Biomol. Chem.*, 2015, **13**, 1860.
- 25 T. Kobashi, Y. Chai, I. Yamada, S. Yamada and M. Tagaya, *Mater. Chem. Phys.*, 2019, **227**, 134; S. Yamada, T. Kobashi and M. Tagaya, *J. Mater. Chem. B*, 2021, **9**, 1896.
- 26 S. Valetti, A. Feiler and M. Trulsson, *Langmuir*, 2017, **33**, 7343.
- 27 I. Izquierdo-Barba, M. Colilla, M. Manzano and M. Vallet-Regí, *Microporous Mesoporous Mater.*, 2010, **132**, 442.
- 28 C. H. Huang, K.-P. Chang, H.-D. Ou, Y.-C. Chiang and C.-F. Wang, *Microporous Mesoporous Mater.*, 2011, **141**, 102; S. Spange, Y. Zimmermann and A. Graeser, *Chem. Mater.*, 1999, **11**, 3245; J. Kecht, A. Schlossbauer and T. Bein, *Chem. Mater.*, 2008, **20**, 7207.

